Electromagnetically induced generation, gain in delayed wave mixing, and measuring coherent states using quantum-interference windows

I. Pop and L. Moorman
Department of Physics and Astronomy, University of Wyoming, Laramie, Wyoming 82071
(Received 2 May 1997; revised manuscript received 6 April 1998)

A three-level atom interacting with classical electromagnetic fields is coherently excited by a two-photon transition near resonance and subsequently makes a second transition driven at resonance by a weak ir field at the noise level. Our calculation predicts generation of an electromagnetic field at a third frequency in the uv from zero field. Calculations show a gain of the uv radiation with propagation through the medium, though the populations of the two levels involved are never inverted. Other calculations produce a pulsed amplifier, two-photon optical nutation, and free induction memory. An effective susceptibility is defined and its imaginary part is found to be a good indicator of mode specific absorption and emission by the atomic state, and its real part a good indicator of dispersion. These calculations exemplify the possibility of coherent control over an atomic vapor and the production of a superradient macroscopic ensemble of states in the retarded frame for realistic parameters. [S1050-2947(98)08808-8]

PACS number(s): 42.50.Gy, 42.65.Sf, 32.80.Bx, 32.80.Qk

I. INTRODUCTION

The effect of the coherence of electromagnetic fields on the production of coherent states of a macroscopic ensemble of three-level atoms is investigated numerically. The first calculation shows the role of coherence in a closed three-level atomic infrared pulse amplifier with a two-photon pump where the energy is stored in the medium and the amplification is mediated by the off-diagonal elements of the density matrix. A second calculation uses the same three-level system prepared by the two-photon pump, which subsequently interacts with two additional near-resonance fields and demonstrates the role of the atomic coherence during such a sequence of interactions. Electromagnetically induced generation of an ultraviolet field from zero is shown to be possible due to the prepared atomic coherence (i.e., a quantum interference). The remaining atomic coherence imposed by the coherent electromagnetic fields, which remains after all interactions have ceased on this nonlinear medium, is investigated. The experimental parameters for a practical case studied in our laboratory suggest that superradiation is possible in the final ensemble of atoms. This coherence of atoms could possibly be applied to produce practical nonlinear devices.

Quantum interferences between various atomic state pathways for excitation or decay through coherently populated atomic eigenstates are a well-known source for angular and temporal cross-section correlations in atomic and nuclear collision spectroscopy, manifested as variations in the correlated signal. Such interferences have been observed using coincidence techniques in various kinds of electron-, atom-, and ion-atom collisions, techniques that were developed in γ-γ correlation experiments in nuclear physics. The degree of coherence of the atomic states is usually evident in nonzero off-diagonal density-matrix elements, depending on the choice of basis [1,2]. Off-diagonal density-matrix elements play also a critical role in the original two-level atomic Rabi model, a simple application of the dynamics of a coherent atomic population driven by an external electromagnetic field, and in propagating pulses through open two-level systems [3]. Recently, increasingly accurate experimental techniques, improved theoretical insight, and enhanced computational capabilities have sharpened interest in the effects of quantum interference of multilevel atoms on pump and probe electromagnetic fields. This has lead to the identification of various subtle quantal phenomena such as dark states, lasing without inversion (LWI), electromagnetically induced transparancy (EIT), and suppression of stimulated hyper-Raman generation [4–8]. In other applications coherent states are studied to find the beneficial effects of collisions in laser-cooled samples, Bose-Einstein condensation (BEC), the production of entangled states, and coherent control of Rydberg states [9–13]. Closely related to the work presented herein on the nonlinear interaction of strong electromagnetic fields with coherent atomic states are the third-harmonic-generation experiments with delayed excitation pulses [14], optical accumulated echo with weak pump pulses [15], and four-wave-mixing processes with time-delayed strong pump pulses [16,17]. These examples show that the quantum interference due to a coherent population of eigenstates with energy transitions in the optical frequency regime has now developed from spectroscopic fundamental observations, allowing us to derive basic quantum-mechanical phenomena about atomic populations, applications of collision kinematics, and even a tool for the construction of sophisticated macroscopic quantum devices.

II. MOTIVATION

In our experiments we are interested in the creation and propagation of different electromagnetic field modes at frequencies internally generated by the medium [18,19]. Here we calculate the interaction of a three-level atom with three classical electromagnetic fields as indicated in Fig. 1. The levels of the sodium atom and relevant electromagnetic fields are selected to provide realistic calculations for our experiments ($|1\rangle = |3S_{1/2}\rangle$, $|2\rangle = |5S_{1/2}\rangle$, and $|3\rangle = |4P_{1/2,3/2}\rangle$). In the experiment, the ground state is coupled via a two-photon transition to state $|2\rangle$. The two excited states $|2\rangle$ and $|3\rangle$ are coupled to each other by an electric-dipole transition via ir

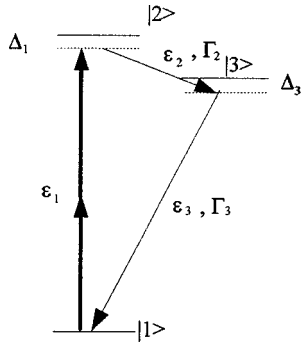

FIG. 1. Qualitative positioning of the energies of the three-level atomic system with three electromagnetic fields ε_i considered. The detunings Δ_i, as indicated, are positive.

radiation and the excited state $|3\rangle$ is coupled back to the ground state $|1\rangle$ by an electric-dipole transition via uv radiation. The numerical values relevant to the system are given in Table I in the Appendix. In the phenomena studied here, the fields are large and the frequencies are close to the atomic resonances. Therefore, the usual nonlinear theory in terms of a perturbative susceptibility is not useful [20,21]. Our study adopts an approach appropriate for strong electromagnetic fields and an optically dense matter field by combining Maxwell's equations for classical fields with the equations for the quantum-mechanical density matrix, an extension of the optical Bloch equations for three-level atoms and three fields.

When all particles are identical and noninteracting, the *N*-particle state can be reduced to a coherent-state one-particle formalism, which we will use throughout the calculations. The reverse is also valid in our case. The coherent electromagnetic field causes coherent atomic excitation of the individual atoms and the *N*-particle density matrix at a given location can be written as a product of the calculated one-particle density matrices. The requirements for this are the following. (i) Velocities of the atoms are small enough so that during the observation time atoms are approximately at one position. (ii) Atomic population decay times and times between inelastic collisions are large compared to the experimental observation times. (iii) Elastic two-atom interactions or multiple-particle interactions, wall effects, and collisions with inert buffer gas particles lead to a coherent dephasing time long compared to the interaction time scale and can be neglected.

After introducing the slowly varying amplitude approximation for electromagnetic fields, the resulting 15-dimensional set of simultaneous first-order differential equations for real functions is solved numerically for transient behavior of the fields and density matrix for a realistic sequence of incident fields and initial conditions of the atoms. The coupled atomic density-matrix–Maxwell equations are solved in one spatial dimension, allowing reshaping of the pump pulse and internal generation of new fields. The solution is relevant for collimated beams or describing fields on the symmetry axis of focused pump beams.

III. PROPAGATION EQUATIONS AND NUMERICAL PROCEDURE

Assuming a homogeneously broadened system, an electromagnetic field linearly polarized along **u** is given by

$$\mathbf{E}(z,t)=\tfrac{1}{2}\mathbf{u}\sum_{q=1}^{3}[\varepsilon_q(z,t)e^{i(k_qz-\omega_qt)}+\text{c.c.}],$$

with $\mathbf{k}_q=k_q\hat{\mathbf{z}}$ in the medium. The three complex fields $\varepsilon_q(z,t)$ with frequencies ω_q, with $2\omega_1=\omega_2+\omega_3$, are regarded as slowly varying in amplitude (envelope) and phase within a period and a wavelength of the carrier wave (slowly varying envelope approximation); hence rapid time and space dependences are contained only in exponentials. The Hamiltonian in the Schrödinger picture $H=H_{\text{at}}+V(t)^{(S)}$, a combination of the atomic Hamiltonian and the dipole atom-field interaction, may be introduced into the equation for the evolution of the density operator $d\rho/dt=-i/\hbar[H,\rho]+\partial\rho_R/\partial t$ with collisional phase relaxation and population transfer phenomenologically included in the last term. The temporal change of an amplitude is slower than the time given by the inverse of any detuning to any intermediate state. This leads to the adiabatic elimination of the intermediate $|3P_{1/2,3/2}\rangle$ state in the two-photon system, except for its contribution to an effective two-photon coupling constant K_{21}.

To transform to a convenient interaction picture, we choose the zeroth-order Hamiltonian $H_0=(E_1+2\hbar\omega_1\delta_{2j}+\hbar\omega_3\delta_{3j})\delta_{ij}$ (no summation convention). The density-matrix and coupling-matrix elements transform by appropriate phase rotation canceling the phase rotations of the negative rotating terms. After integration of the equations over a period of the rapidly oscillating terms, we are left with only terms varying slowly in time rotating-wave approximation (RWA):

$$d\rho_{11}/dt=\Gamma_3\rho_{33}-i/\hbar(V_{12}\rho_{21}+V_{13}\rho_{31}-\rho_{12}V_{21}-\rho_{13}V_{31}), \tag{1a}$$

$$d\rho_{22}/dt=-\Gamma_2\rho_{22}-i/\hbar(V_{21}\rho_{12}+V_{23}\rho_{32}-\rho_{21}V_{12}-\rho_{23}V_{32}), \tag{1b}$$

$$d\rho_{33}/dt=\Gamma_2\rho_{22}-\Gamma_3\rho_{33}-i/\hbar(V_{31}\rho_{13}+V_{32}\rho_{23}-\rho_{31}V_{13}-\rho_{32}V_{23}), \tag{1c}$$

$$d\rho_{21}/dt=-(\gamma_{21}+i\Delta_1)\rho_{21}+i/\hbar(\rho_{23}V_{31}-V_{23}\rho_{31})+i/\hbar V_{21}(\rho_{22}-\rho_{11}), \tag{1d}$$

$$d\rho_{23}/dt=-(\gamma_{23}+i\Delta_2)\rho_{23}+i/\hbar(\rho_{21}V_{13}-V_{21}\rho_{13})+i/\hbar V_{23}(\rho_{22}-\rho_{33}), \tag{1e}$$

$$d\rho_{31}/dt=-(\gamma_{31}+i\Delta_3)\rho_{31}+i/\hbar(\rho_{32}V_{21}-V_{32}\rho_{21})+i/\hbar V_{31}(\rho_{33}-\rho_{11}). \tag{1f}$$

The coupling strengths are given by $K_{21}=(1/2\hbar)\Sigma_{j=1}^{4}[\mu_{2j}\mu_{j1}/(\omega_{2j}-\omega_1)]$ [22], $V_{21}=K_{21}\varepsilon_1^2/2$, $V_{31}=-\mu_{31}\varepsilon_3/2$, and $V_{23}=-\mu_{23}\varepsilon_2/2$. ω_1 is the laser frequency and the detunings are $\Delta_1=\omega_{21}-2\omega_1$, $\Delta_2=\omega_{23}-\omega_1$, and $\Delta_3=\omega_{31}-\omega_3$. Conservation of energy requires that $2\omega_1=\omega_2+\omega_3$ and hence test $\Delta_1=\Delta_2+\Delta_3$ [23].

The coupling of the atom to the electromagnetic field is described by the Maxwell equations for the field amplitudes ε_q. We transform to the retarded frame for forward-propagating waves where $\tau=t-z/c$ and $\zeta=z$. Maxwell's equations using the slowly varying envelope approximation become $\partial\varepsilon_q/\partial\zeta=i(k_q/2\varepsilon_0)P_q$, with $q=1,2,3$ and ε_0 the permittivity of free space. The modes of polarization P_q are given by off-resonance and resonant contributions

[22,24,25]. This model neglects the slowly varying, linear, background susceptibility due to nonresonant states in the atomic vapor. The dominant contribution for the field mode ε_1 is the polarization caused by the single-frequency off-resonance polarizability, which is bilinear, antilinear in the amplitude of the pump mode of the field, and linear in the density-matrix element $P_1=-4NK_{21}\rho_{21}\varepsilon_1^*$, with N the atomic density. The dominant contributions to the fields ε_2 and ε_3 are the polarizations caused by the resonant polarizabilities, which are only linear in the off-diagonal density-matrix elements $P_2=2N\mu_{32}\rho_{23}$ and $P_3=2N\mu_{13}\rho_{31}$, where the electric-dipole elements are assumed real. The equations for the fields are then

$$\partial\varepsilon_1/\partial\zeta=ik_1(N/\varepsilon_0)(-2K_{21}\rho_{21}\varepsilon_1^*), \tag{2a}$$

$$\partial\varepsilon_2/\partial\zeta=ik_2(N/\varepsilon_0)\mu_{32}\rho_{23}, \tag{2b}$$

$$\partial\varepsilon_3/\partial\zeta=ik_3(N/\varepsilon_0)\mu_{13}\rho_{31}, \tag{2c}$$

where the off-diagonal density-matrix elements provide coherent sources and sinks for the three radiation fields. In equations for the density matrix, derivatives with respect to τ shall replace derivatives by t.

The coupled equations (1) and (2) are successively solved for each position ζ by integrating over τ via the Runge-Kutta-Fehlberg fifth-order method with adaptive temporal step size. The boundary conditions are given by the fields sent into the face of the medium ($\zeta=0$) and determined by an initial condition where the atoms are in the ground state for each ζ at $\tau=0$. In our numerical calculations the truncated Gaussian electric field ε_1 has its center at $\tau=2$ ns, a real amplitude of 2×10^7 V/m, a rms width of 1 ns, and a pulse duration of 2 ns. The ir field ε_2 is chosen to have two temporal shapes: (i) a hyperbolic-secant pulse with its center at $\tau=4$ ns, a real amplitude of 2×10^5 V/m, and full width at half maximum of 2.634 ns and (ii) a noise field that has a constant amplitude of 1.78×10^{-2} V/m. The uv field ε_3 is taken to have the initial values of (i) a noise field that has a constant amplitude of 5.8×10^{-2} V/m or (ii) zero-amplitude field. For times $\tau<2$ ns the fields ε_2 and ε_3 have zero amplitude. The number density of the medium is $N=8.7\times10^{19}$ m^{-3}.

From the polarization $P(z(\zeta,),t(\zeta,\tau))=\Sigma_q P_q(\zeta,\tau)e^{-i\omega_q t}$ we may define a slowly varying effective susceptibility for each mode q as a function of ζ and τ, $\chi_q(\zeta,\tau)=P_q(\zeta,\tau)/[\varepsilon_0\varepsilon_q(\zeta,\tau)]$. Introducing this effective susceptibility into the equations for the slowly varying envelope and integrating yields

$$\varepsilon_q=C_q\ \exp\left\{\varphi_q^0+i(k_q/2)\int\chi_q d\zeta\right\}, \tag{3}$$

where C_q and are φ_q^0 are real. Hence the modulus is given by $|\varepsilon_q|=\exp\{-(k_q/2)\int \mathrm{Im}(\chi_q)d\zeta\}$ and the phase as $\varphi_q=\varphi_q^0+(k_q/2)\int \mathrm{Re}(\chi_q)d\zeta$. When ε_q goes through zero, a phase contribution π must be added or subtracted. The imaginary part of the effective susceptibility describes absorption of the electromagnetic field if it is positive and amplification if it is negative. The real part causes advancement or retardation of the phase relative to propagation through vacuum, a dispersive effect. Introduction of the effective susceptibility provides a convenient and efficient means for describing the behavior of the electromagnetic field versus ζ at fixed τ, though it does require a complete solution valid in the neighborhood of ζ.

IV. THREE-LEVEL ATOMS INTERACTING WITH A SEQUENCE OF PULSES OF VARIOUS FREQUENCIES

A. Preparation of the coherent state, optical nutation, and free induction memory

Figures 2(a) and 2(b) show the consequence of sending only the strong Gaussian truncated pump pulse at ω_1 with detuning Δ_1 switched off at 2 ns into the medium. In Fig. 2(a) we show the pump pulse $\varepsilon_1(\tau)$ propagated through 4.375 cm of the medium. By subtracting the initial Gaussian pulse shape of the amplitude and magnifying the difference, the figure shows an oscillation in amplitude near the peak of the pulse whose frequency and amplitude increase with increasing pulse power. The amplitude of this oscillation exactly reproduces the shape of the amplitude of the initial pump pulse. These increases in frequency and amplitude and the congruency in shape of its envelope with the initial pump pulse are unique consequences of the two-photon coupling between states $|1\rangle$ and $|2\rangle$. These occur because the polarization in the source of Maxwell's equation (2a) is proportional to the pump field ε_1^* as well as the off-diagonal matrix element ρ_{21}. This behavior is distinctly different from that of one-photon coupling, which would show only an increasing frequency but a constant amplitude. This oscillation results from an interference between the propagating electromagnetic field and the field caused by the polarization at ω_1 and is an example of two-photon optical nutation.

Figure 2(b) shows the complex density-matrix element ρ_{21} that indicates the coherence between the ground state $|1\rangle$ and the exited state $|2\rangle$. While the preparatory truncated Gaussian pump pulse grows, it creates an oscillatory behavior increasing in frequency of the imaginary part of ρ_{21} and develops a positive average value of the real part with an oscillation superimposed. The oscillatory frequency corresponds to the generalized Rabi frequency $\Omega'=(|\Omega|^2+\Delta_1^2)^{1/2}$, which increases with increasing amplitude of the pump ε_1^* until it is truncated at 2 ns [26]. Our calculation of the effective susceptibility for ε_1 has three regions of negative imaginary values in the first 2 ns that correspond exactly to the three regions where the power in the field increased compared to its initial pump power, the local maxima visible in Fig. 2(a).

Figure 2(b) shows a strong oscillating off-diagonal element after the pump pulse is switched off. After $\tau=2$ ns the system is left in a coherently excited state in general described by

$$\rho(z,\tau)=\tfrac{1}{2}\begin{pmatrix}1 & e^{i[\varphi+\Delta(\tau-2)]}\\ e^{-i[\sigma+\Delta(\tau-2)]} & 1\end{pmatrix}.$$

This is consistent with a zero phase difference at $\tau=2$ ns. The large oscillations in Fig. 2(b) describe the phase rotation on this basis and does not reflect population changes. Although the pump pulse is turned off, the observed frequency corresponds exactly to the detuning of the pump pulse frequency from that of the two-photon atomic resonance. This effect is a memory of the coherent pump pulse stored in the

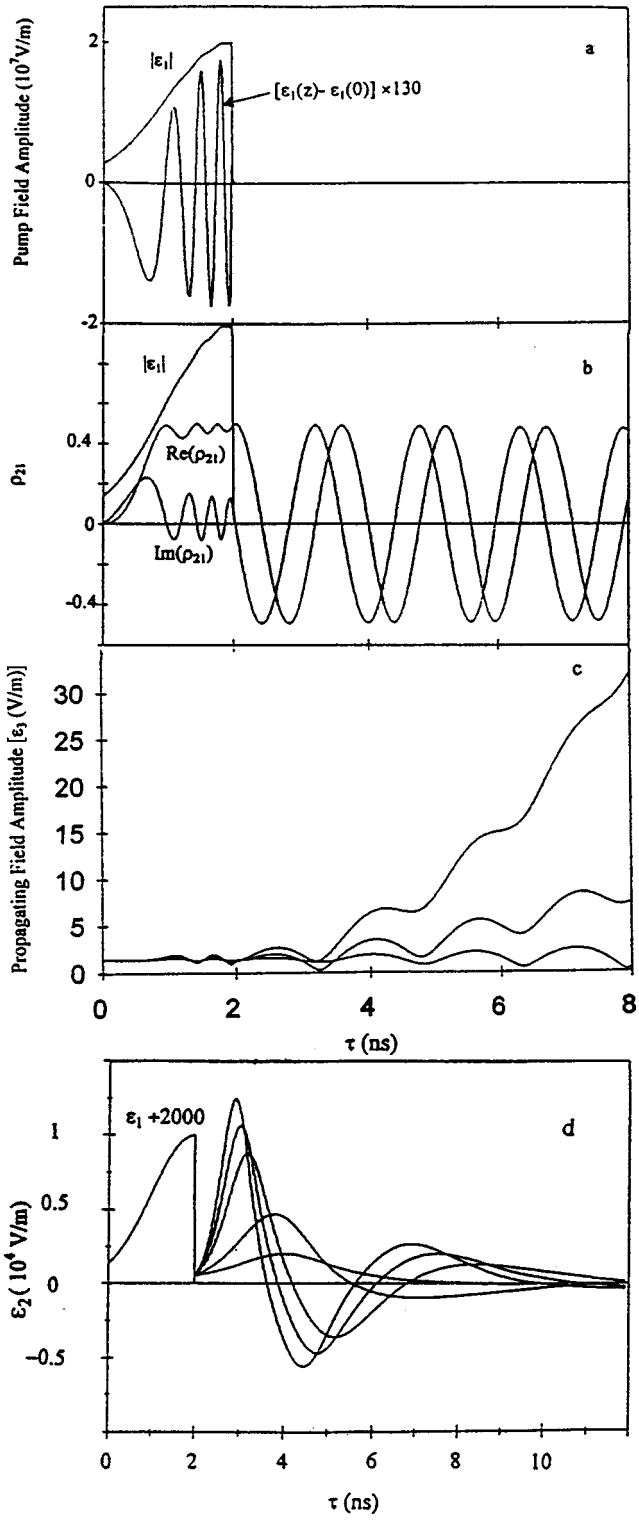

FIG. 2. (a) Half-Gaussian pump pulse with $\varepsilon_{1,\max}=2\times10^7$ V/m propagated through the active medium with a density of $N=8.7\times10^{19}$ atoms/m^3 to $z=4.375$ cm. Interference oscillations are visible on top of the propagated pump pulse. After subtraction of the incident pulse and enhancing for graphing appropriately, the oscillations are clear with an increasing frequency and an amplitude envelope that is congruent to the original pump pulse. (b) Off-diagonal density-matrix element of states $|1\rangle$ and $|2\rangle$. The pump pulse induces fast oscillations in real and imaginary parts while it is nonzero, but when turned off ($\tau>2$ ns) the oscillatory behavior persists, although with a lower frequency. The calculation indicates that the atoms occupy a coherent state. This oscillation represents two-photon optical nutation ($\tau<2$ ns) and free induction memory ($\tau>2$ ns) with their characteristic frequencies, the generalized two-photon Rabi frequency and detuning, respectively. (c) Possible measurement of the free induction memory. The uv field ε_3 at $z=3.3$ μm, shown as the smallest amplitude in this graph, shows beats with the generated intensity through the $|1\rangle$-$|2\rangle$ polarization coupled with the ir field ε_2. When the fields propagate further in the medium, as shown by the larger amplitudes corresponding to $z=9.8$, 16.3, and 20 μm, the beat oscillation amplitude increases above the initial level and gain is expected. (d) A three-level closed-system calculation of propagating field amplitude for the field ε_2. A weak hyperbolic-secant pulse ε_2 is sent into the sodium and amplified. $z=0$, 12.5, 37.5, 50, and 62.5 μm.

atomic coherence of the medium and is the free induction decay of the atomic polarization. Since the times for population decay to other states and collision dephasing are much longer than the time scale of the calculation, as shown by the figures, we shall refer to this effect as free induction memory of the polarization.

B. Interference measurements

The free induction memory may be ''read out'' without significantly destroying it by a weak electromagnetic field of the same detuned frequency as the pump field. Calculations show this effect by switching the pump down to low power [27]. Interference between the weak propagating field and the polarization produces an oscillation in field intensity at the generalized Rabi frequency. The field does not destroy the polarization appreciably in the calculated time window. This oscillation can be understood as the coupling of the coherence matrix element with the amplitude of the pump field via $\rho_{21}\varepsilon_1^*$. In the experiment the quantum-mechanical phase between the population of upper state and ground state can be calculated by extrapolating the measured oscillations

to the moment at which the Gaussian pulse is switched off. This method may be an advantage over a direct method because the frequency of the optical nutation, during the creation of this coherence for times shorter than 2 ns, can be many orders of magnitude greater than the detuning.

It is also possible to read out the free induction memory by introducing a noise field with zero detuning on the $|2\rangle$-$|3\rangle$ transition and a third field near the $|3\rangle$-$|1\rangle$ transition. In that case the oscillations are not directly observed with the second resonant field ε_2, but are induced onto the third field ε_3. This oscillation in the third field is shown in Fig. 2(c) and is clear at all times for a short distance into the medium. The same figure shows how gain tends to obscure the free induction memory as fields propagate more deeply into the medium.

C. A closed-system, three-level propagating pulse amplifier

After the Gaussian pump pulse for the ε_1 field, a weak pulse ε_2, shaped as a hyperbolic secant centered at 4 ns, is sent into the medium at the ir transition. Figure 2(d) shows both the truncated pump pulse ε_1 propagated to some distance into the medium and the weak hyperbolic-secant pulse $|\varepsilon_2|$ propagated to several distances, significantly enhanced due to the induced polarization of the atomic medium. The propagating ε_2 pulse experiences an amplification of the pulse power and 180° phase changes in the amplitude. The pulse shape for ε_2 in Fig. 2(d) qualitively resembles that for the open two-level continuously and incoherently pumped pulse amplifier studied by Icsevgi and Lamb [3] as shown in their Fig. 27. The pulse area, or phase $\phi = \int \Omega \, dt$, and integrated energies as a function of the distance in the medium were also calculated. The pulse area smoothly increases towards 2.8, somewhat short of π, which is expected but still with a positive slope, and the integrated pulse energy shows that the system has a linear gain in power.

The amplification in our three-level amplifier can be understood as follows. As before, a coherent field pump pulse creates an atomic coherent state of the free-field eigenstates $|1\rangle$ and $|2\rangle$. In addition, an inversion between states $|2\rangle$ and $|3\rangle$ builds during the preparatory pump pulse $[(\rho_{22}-\rho_{33}) > 0]$. Both persist after the pump pulse is truncated. Injection of a probe pulse with amplitude ε_2 makes V_{23} large, allowing a growth of ρ_{23} mainly through the term $V_{23}(\rho_{22} - \rho_{33})$ in Eq. (1e) as long as the inversion between states $|2\rangle$ and $|3\rangle$ persists. Thus the Maxwell equation for the field ε_2 [Eq. (2b)] has the off-diagonal density matrix element ρ_{23} as a source that creates a contribution to the probe field that can sometimes amplify and sometimes attenuate its amplitude leading to the constructive and destructive interference as the pulse energy grows while traveling through the medium.

D. Atomic state population and electromagnetic field dynamics

Figures 3(a)–3(d) show the full quantal interaction of a three-level atom with a sequence of two pulses and a third field at a noise level. The same truncated Gaussian pulse prepared the initial coherent state. A second pulse at ω_2 with a hyperbolic-secant envelope with its maximum at 4 ns (not shown) and a third noise field at ω_3 are turned on at 2 ns. The full quantal dynamics of atomic state and fields are shown after propagating 19.53 μm through the medium. In Fig. 3(a) we show the populations of the three states oscillating with the generalized Rabi frequencies. The electric-field amplitudes are normalized and shown for reference.

The calculations for times below 2 ns also show the population oscillations in ρ_{11} and ρ_{22} due to interferences of the dressed atomic states $|+\rangle$ and $|-\rangle$ of the normal Rabi model built by symmetric and antisymmetric combinations of the bare atomic states $|1\rangle$ and $|2\rangle$ [18]. The special feature here is that the atomic population is moved back and forth by a two-photon transition and thus the calculation describes the process of absorption and reemission of two simultaneous photons of frequency ω_1. The population of the excited state ρ_{22} would have reached zero on each oscillation if the frequency of field ε_1 had been exactly on the two-photon resonance for states $|1\rangle$ and $|2\rangle$.

Calculations show that, as the pump pulse propagates, inversion of the population is created and the nonlinear polarization amplifies a second field ε_2, which becomes large enough to create a Rabi oscillation for the population of states $|2\rangle$ and $|3\rangle$. This reverses the populations seen near 3 ns in Fig. 3(a). Between 3 and 3.7 ns the population of $|3\rangle$ increases over that of $|2\rangle$ while the amplitude of the ε_2 field also increases, indicating a storage of energy in the electromagnetic field. Thus the energy stored in the atomic system is transferred to the electromagnetic field. From 3.7 to 4.4 ns the reverse takes place. As the electromagnetic field loses energy, it is stored back into the atomic system. Calculations to larger distances show that these Rabi oscillations become more frequent and shift to earlier times as the pulse propagates through the medium.

E. Off-diagonal elements of the density matrix: Population beats, 180° phase flips

Comparing Fig. 3(a) with Fig. 3(b), the maxima in the second electromagnetic field ε_2 coincide with extra beats in ρ_{21} and the latter differs from Fig. 2(b) because of the presence of ε_2. The evolution of the ρ_{23} matrix element is given in Fig. 3(c), showing zeros in the absolute value near the maxima of the ε_2 field. These zeros occur because the ρ_{22} matrix element goes through a minimum at that time where the remaining small amount in Fig. 3(a) is the *incoherent* contribution to that state due to population decay from state $|2\rangle$. This incoherent contribution can easily be recognized at the two minima visible at 3.5 and 6.5 ns, although its growth is slowed down somewhat because state $|2\rangle$ is not populated to such high values during the intermediate times as in the first 3.5 ns. Thus the nodes in ρ_{23} in Fig. 3(c) represent the nodes of the evolution of the coherent part only of the superposed population of the bare eigenstates $|2\rangle$ and $|3\rangle$.

In Fig. 3(d) we show a combination of real and imaginary parts of ρ_{31}, the real and imaginary parts of the amplitude of relevant field mode ε_3, and its field envelope $|\varepsilon_3|$. The ''chasing'' of the various components, 90° out of phase, are an indication of the large atomic coherence that is induced and remains present during the interaction and generation of the field.

F. Effective susceptibilities: Absorption by atoms, dispersion, and gain for fields

A negative value of the imaginary part of the effective susceptibility $\mathrm{Im}(\chi_q)$ indicates an increase of the modulus

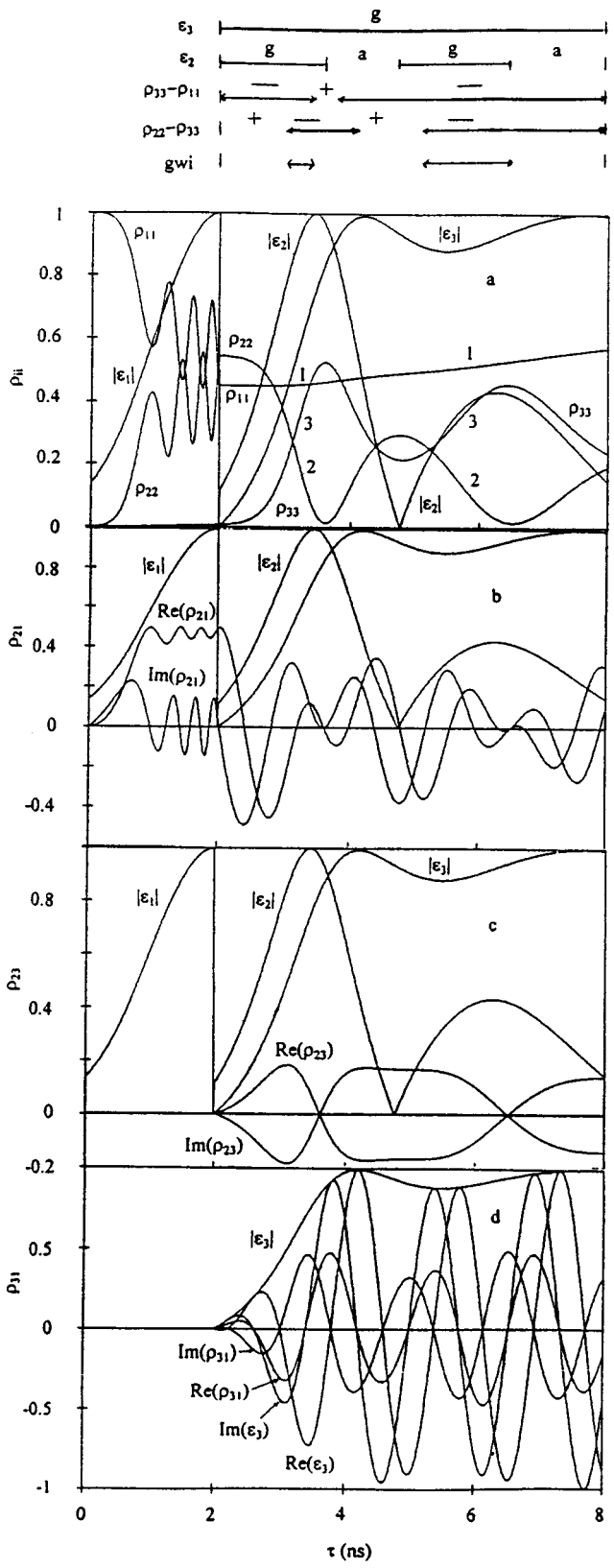

FIG. 3. Complete three-level atom calculation interacting with a sequence of two pulses: a half-Gaussian pulse ε_1 and a subsequent hyperbolic-secant pulse ε_2 [with $\varepsilon_{2,\max}(z=0)=2000$ V/m], and the third field at the noise level. All fields have their maximum rescaled to unity to emphasize their qualitative behavior compared to the density-matrix elements ($\varepsilon_{2,\max}=6768$ V/m and $\varepsilon_{3,\max}=3337$ V/m). (a) Populations and field amplitudes. (b)–(d) Real and imaginary components of ρ_{21}, ρ_{23}, and ρ_{31} compared with field amplitudes. (d) The phase rotation of the ε_3 amplitude has the same angular frequency as the detuning of the two photon pump Δ_1. For the meaning of the arrows above the figure see the text. *g* denotes gain, *a* attenuation; the plus sign inversion, the minus sign a normal population distribution, and gwi gain without inversion ($z=19.53$ μm).

$|\varepsilon_q(\zeta,\tau)|$ for increasing $\zeta=z$ at the same retarded time $\tau=t-z/c$ as described by Eq. (3). The realization that the effective susceptibility is linked to changes in the field amplitude with increasing position ζ at the same time τ and not with increasing τ at the same ζ is essential in interpreting its significance.

The atomic effective susceptibility for the mode ε_3 is shown in Fig. 4(a). It has zero real part, indicating the absence of dispersion and only a negative imaginary part between 2 and 8 ns. Therefore, the field gains energy and the modulus of this amplitude grows as ζ increases. We show the amplitudes for increasing distances ζ in Fig. 4(b), as the field propagates through the medium. The power in the third field ε_3 is increasing in ζ even when the field is decreasing in retarded time in Fig. 3(a). This is not a contradiction because the atoms emit light into the retarded time frame and the

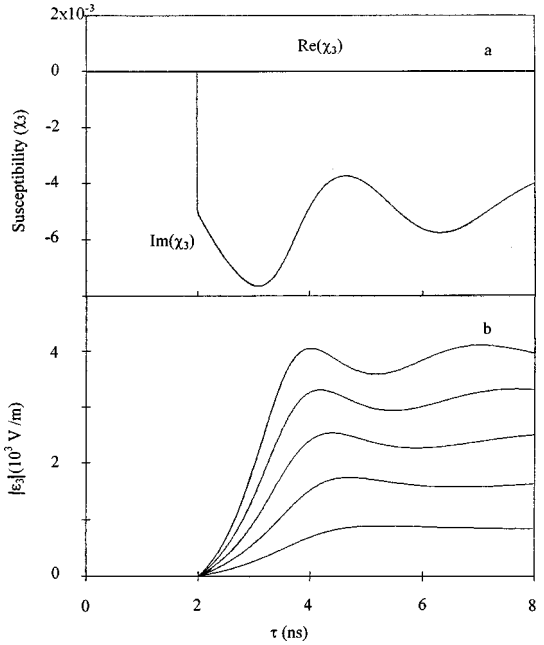

FIG. 4. (a) Effective susceptibility, χ_3 ($z=19.53\ \mu$m). (b) uv field amplitude $|\varepsilon_3|$ for increasing distance ($z=4.88$, 9.77, 14.70, 19.53, and 24.40 μm correlates with increasing amplitudes $|\varepsilon_3|_{\max}$).

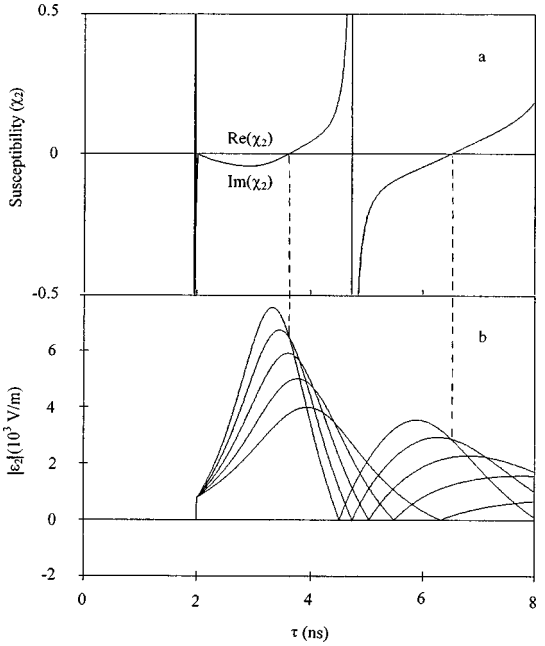

FIG. 5. (a) Effective susceptibility, χ_2 ($z=19.53\ \mu$m). (b) ir field amplitude $|\varepsilon_2|$ for increasing distance ($z=4.88$, 9.77, 14.70, 19.53, and 24.40 μm correlates with increasing amplitudes $|\varepsilon_2|_{\max}$).

energy moves with the wave while the atom stays behind at the same position z. During 93.5% of the calculated time interval for which the ε_3 field has gain, the populations of states $|1\rangle$ and $|3\rangle$ are not inverted as indicated by combining the first and third line segments above Fig. 3(a). Thus ε_3 undergoes gain without inversion.

The advantage of introducing the effective susceptibilities is more evident in the complicated behavior for the second field ε_2 as shown in Fig. 5(a). Two regions of emission with negative $\mathrm{Im}(\chi_2)$ are separated by a region with positive $\mathrm{Im}(\chi_2)$ and again no dispersion $[\mathrm{Re}(\chi_2)=0]$ is found for this mode over most of the region. An instantaneous reversal of susceptibility near 4.74 ns corresponds with a nearly zero value of the field amplitude where it makes a π phase change and indicates the atom changes from absorptive to emissive for this mode. Upon closer scrutiny near 4.74 ns, $\mathrm{Re}(\chi_2)$ is found to rise to a small but finite value over about 10 ps, which is responsible for the π phase change of the field ε_2. Similarly, the two zeros in the susceptibility with positive slope indicate moments at which the atom transforms from emissive to absorptive for the field ε_2. Again, this can be compared with Fig. 5(b) for the fields. During 31.3% of the time interval 2–8 ns, there is gain in the field ε_2 without having inversion between states $|3\rangle$ and $|2\rangle$, which follows from combining the second and fourth line segments above Fig. 3(a). Combining all segments shows 26.9% of the time interval both fields have gain, while none of the level pairs of the three-level atomic states are inverted. These calculations show that, during a coherent process, an atom with a normal population can cause gain without inversion a sizable fraction of the time.

The gain occurs because a matter wave carrying energy, as described by the density-matrix equation (1), is produced in the medium and mixes with the ir light wave to generate and amplify uv light. The energy for the amplification process comes from the atomic system, as was shown in Fig. 4(a). Thus the energy stored in the radial motion of the electrons inside the atoms is converted to the field in two modes simultaneously. The gain process is unlike a parametric process or a Raman laser, where the energy is instantaneously converted from one field to the other, but results from a transfer of energy from the atoms to the field as discussed in [28,29].

The effect on the free induction memory of introducing a faster dephasing rate between the states was studied. For a collision rate of 0.5 ns^{-1} our calculations show a rapid decrease in $|\rho_{31}|$ and decay of the effective susceptibility and field amplitude over the 2–8 ns time interval compared to Figs. 4(a) and 4(b).

Our system differs from others on matter-field mixing [14–16] in three aspects. First, we solve the coupled matter-

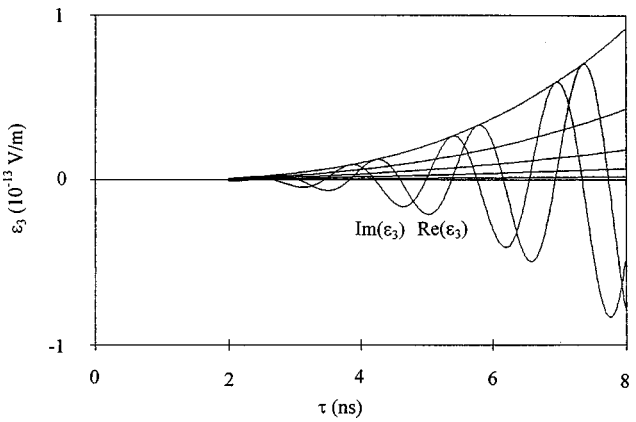

FIG. 6. Electromagnetically induced generation of the uv field (ε_3) by an ir field (ε_2) subsequent to a pump field. Shown is the exponential growth of the uv field from zero as a function of the retarded time for different positions ($z=4.88$, 9.77, 14.56, 19.53, and 24.41 μm) and the real and imaginary components for one (24.41 μm).

field equations and therefore calculate effects of propagation in the forward direction. Second, our matter wave is a coherent atomic wave but not a polarization wave. The matter wave consists of a pure atomic $3S$-$5S$ radial motion as the atom swells and shrinks, maintaining its spheroidal symmetry. Thus the individual atoms do not obtain a static or dynamic dipole moment for the $|1\rangle$-$|2\rangle$ transition during their evolution and no macroscopic polarization is generated in the matter wave of the medium for this transition. Nevertheless, transition dipoles for $|2\rangle$-$|3\rangle$ and $|3\rangle$-$|1\rangle$ still produce corresponding macroscopic dipole waves. In [17] an S-S wave is also considered, but partially overlapping pulses are studied, whereas our preparatory field ε_1 is completely turned off when ε_2 arrives. Third, a difference-wave mixing between an atomic matter wave and an electromagnetic wave is being investigated. In [14–16], sum-frequency generation is studied.

V. ELECTROMAGNETICALLY INDUCED GENERATION

We have calculated generation of an electromagnetic field from zero. The atomic state is prepared again by a truncated Gaussian pulse and the field ε_2 is inserted at the noise level while ε_3 is kept zero until the pump pulse is turned off. Figure 6 shows the generated electromagnetic field ε_3. The creation of field ε_3 has its source in the off-diagonal term ρ_{31} via Eq. (2c), which itself obtains a nonzero value by the action of the term $-iV_{32}\rho_{21}$ in Eq. (1f). This generation of a field results from an electromagnetic wave mixing with the prepared free induction memory discussed before. In Fig. 6 we show the exponential growth of the modulus of the generated field at the onset as a function of retarded time for different positions and the real and imaginary parts of the amplitude for the largest propagation distance. Our calculations also show an exponential amplification of the modulus as a function of position in the medium, which is the characteristic of a true amplifier. The corresponding effective susceptibilities show a strong amplification for the field ε_2 and a weaker gain for the field ε_3.

The uv light generated is not spontaneous emission because the intensity depends on the square of the atomic density and the electromagnetic fields are classical. It is also not stimulated emission because no uv photons have to be present to start the generation and the uv light is generated without population inversion for the corresponding levels. It is also not traditional four-wave mixing since no visible pump field is present simultaneously.

VI. COHERENCE OF THE FINAL STATE

Our single-particle density matrices allow the calculation of a superradient state for a large number of atoms. Under the assumptions discussed in Sec. II, without loss of generality we can construct the N-particle density operator from the single-atom matrices calculated in the previous sections. This operator in terms of our calculated matrices in the interaction picture is then

$$R(N)^{(I)}=\sum_{i_1\cdots i_N}^{3\cdots 3}\rho^{(1)}_{i_1j_1}\rho^{(2)}_{i_2j_2}\cdots\rho^{(N)}_{i_Nj_N}|i_1i_2\cdots i_N\rangle^{II}\langle j_1j_2\cdots j_N|.$$

Each atom is in the ground state $|1\rangle$ before the preparatory pulse reaches it and has a quantal phase rotation based on its energy and a fixed absolute phase contribution. The N-particle density operator of the initial ground-state system for atoms at a position ζ is thus $R(N)=|11\cdots1\rangle\langle11\cdots1|$. If we send a π pulse through the atomic system for the two-photon transition, each atom would make the transition to $|2\rangle=|5S\rangle$. The final density operator is $R(N)^{(I)}=|22\cdots2\rangle\langle22\cdots2|$ describing a superradiating state that allows an anisotropic radiation pattern [30].

The medium may be left with a free induction memory that translates into a position-dependent index of refraction. For the pulse amplifier as shown in Fig. 2(d), we found that a well calculable phase rotation exists after a sequence of two pulses passed it. The refraction written onto the medium could next be used for the scattering of relatively weak electromagnetic waves at different frequencies.

ACKNOWLEDGMENTS

We thank Professor G. A. Rebka, Jr., Professor R. Inguva, and Dr. A. B. Ritchie for their interest, encouragement, and helpful comments.

APPENDIX

The numerical values used in our calculations are summarized in the following table (Table I).

TABLE I. Numerical values used in our calculations.

ij	n		λ (nm)	$\lvert\mu_{ij}\rvert$[a] (a.u.)	$\lvert\mu_{ij}\rvert$[a] (m C)	Γ_n (μs^{-1})	γ_{ij} (μs^{-1})	Δ_q (rad/ns)	R_{coll}[b] (ns^{-1})
21	1	$5S$-$3S$					6.4[d]	$\Delta_1=4$	0.5
23	2	$5S$-$4P$[c]	3412.5	5.92	5.0188×10^{-29}	12.77[d]	7.92[d]	$\Delta_2=0$	0.5
31	3	$4P$-$3S$	330.24	0.235	1.9922×10^{-30}	3.08[d]	1.55[d]	$\Delta_3=4$	0.5
24		$5S$-$3P$	615.85	0.528	4.4761×10^{-29}	7.2			
41		$3P$-$3S$	589.19	2.51	2.51×10^{-29}	62.9			

[a]Values from Miles and Harris [31]. The two-photon coupling constant is $K_{21}=-6.1617\times10^{-30}$ C m^2/V. No differences were observed in the results when positive or negative dipole matrix elements were used for $4P$-$3S$ and $5S$-$4P$ [32,31]. Positive values are used throughout.

[b]Only when applicable. The calculated collision dephasing time is longer than the pulse duration when buffer gas pressures of less than 20 Torr are used in our experiment.

[c]Statistical averaging of fine-structure multiplet level energies is used: $E=(4E_{3/2}+2E_{1/2})/6$.

[d]$A(5S,3P)$, $A(5S,4P)$, $A(4P,3S)$, and $A(4P,3D)$ are combined from atomic transition probabilities given in [33] to generate the decay and the dephasing rates according to the formulas $\Gamma_n=\Sigma_m A_{nm}$ and $\gamma_{ij}=(\Gamma_i/2+\Gamma_j/2)+R_{\text{coll}}$. The values of the Γ_n and γ_{ij} presented in the table are for $R_{\text{coll}}=0$.

[1] L. Moorman, J. van Eck, G. Nienhuis, and H. G. M. Heideman, J. Phys. B **24**, 3771 (1991); **18**, 4707 (1985). Many other examples can be found in *Coherence and Correlation in Atomic Collisions*, edited by H. Kleinpoppen and J. F. Williams (Plenum, New York, 1980).
[2] K. Blum, *Density Matrix Theory and Applications* (Plenum, New York, 1981).
[3] A. Icsevgi and W. E. Lamb, Jr., Phys. Rev. **185**, 517 (1969).
[4] U. Gaubatz, P. Rudecki, M. Becker, S. Schiemann, M. Kulz, and K. Bergmann, Phys. Rev. Lett. **149**, 463 (1988).
[5] S. E. Harris, Phys. Rev. Lett. **62**, 1033 (1989); M. O. Scully, S.-Y. Zhu, and A. Gavrielides, *ibid.* **62**, 2813 (1989).
[6] K. J. Boller, A. Imamoglu, and S. E. Harris, Phys. Rev. A **66**, 2593 (1991); J. E. Field, K. H. Hahn, and S. E. Harris, *ibid.* **67**, 3062 (1991); A. Kasapi, M. Jain, G. Y. Yin, and S. E. Harris, Phys. Rev. Lett. **74**, 2447 (1995).
[7] W. R. Garrett, Phys. Rev. Lett. **70**, 4059 (1993); L. Deng, W. R. Garrett, J. Y. Zhang, and M. G. Payne, Phys. Rev. A **52**, 489 (1995); W. R. Garrett, M. A. Moore, R. C. Hart, and M. G. Payne, *ibid.* **45**, 6687 (1992); M. G. Payne, J. Y. Zhang, and W. R. Garrett, *ibid.* **48**, 2334 (1993).
[8] P. Zhou and S. Swain, Phys. Rev. Lett. **78**, 832 (1997).
[9] L. Marcassa *et al.*, Phys. Rev. Lett. **73**, 1191 (1994); D. J. Heinzen, in *Quantum Computation*, edited by D. Wineland, C. E. Wieman, and S. J. Simth, AIP Conf. Proc. No. 323 (AIP, New York, 1995), p. 369.
[10] A special collection of papers on these topics can be found in *Laser Manipulation of Atoms and Ions*, Proceedings of the International School of Physics ''Enrico Fermi,'' Course CXVIII, Varenna, 1991, edited by E. Arimondo, W. D. Phillips, and E. Strumia (Elsevier, Amsterdam, 1992); S. Stenholm, *ibid.*, p. 29; C. Cohen-Tannoidji, *ibid.*, p. 99; G. Nienhuis, *ibid.*, p. 171; E. Arimondo, *ibid.*, p. 191; W. D. Phillips, *ibid.*, Introduction.
[11] M. H. Anderson, J. R. Ensher, M. R. Matthews, C. E. Wieman, and E. A. Cornell, Science **269**, 198 (1995); C. C. Bradley, C. A. Sackett, J. J. Tollett, and R. G. Hulet, Phys. Rev. Lett. **75**, 1687 (1995); K. B. Davis, M. O. Mewes, M. R. Andrews, N. J. van Druten, D. S. Durfee, D. M. Kurn, and W. Ketterle, *ibid.* **75**, 3969 (1995).
[12] A. Eckert, in *Quantum Computation* (Ref. [9]), p. 450.
[13] C. R. Stroud, Jr., in *Quantum Computation* (Ref. [9]), p. 336.
[14] C. Tai, Phys. Rev. A **23**, 2462 (1981).
[15] S. Asaka, H. Nakatsuka, M. Fujiwara, and M. Matsuoka, Phys. Rev. A **29**, 2286 (1984); N. Morita and T. Yajima, *ibid.* **30**, 2525 (1984).
[16] R. Beach, D. DeBeer, and S. R. Hartmann, Phys. Rev. A **32**, 3467 (1985); S. R. Hartmann and J. T. Manassah, J. Phys. B **23**, 1363 (1990).
[17] T. Nakajima, Opt. Commun. **110**, 620 (1994).
[18] L. Moorman and I. Pop (unpublished).
[19] I. Pop, G. A. Rebka, and L. Moorman (unpublished).
[20] R. W. Boyd, *Nonlinear Optics* (Academic, New York, 1992).
[21] N. B. Delone and V. P. Krainov, *Atoms in Strong Light Fields* (Springer-Verlag, Berlin, 1985).
[22] A. Guzman de Garcia, P. Meystre, and R. R. E. Salomaa, Phys. Rev. A **32**, 1531 (1985); A. Guzman de Garcia, Ph.D. thesis, Max Planck Institute für Quanten Optik, 1984.
[23] The population decay times are related to the population decay rates by $T_1=1/\Gamma_2$ and the dephasing times are related to the dephasing rates by $T_2=1/\gamma_{21}$. Also both one-photon and two-photon Rabi frequencies are given by $\Omega_{ij}=2V_{ij}/\hbar$.
[24] J. R. Ackerhalt, P. D. Drummond, and J. H. Eberly, in *Coherence, Cooperation and Fluctuations*, edited by F. Haake, L. M. Narducci, and D. Walls (Cambridge University Press, Cambridge, 1986), p. 104.
[25] B. W. Shore, *The Theory of Coherent Atomic Excitation Volume 1* (Wiley, New York, 1990), Sec. 12.2.
[26] Factor of 2 differences can be found in the literature. We define the Rabi frequency as the frequency of the atomic population change of a low-density atomic sample irradiated by a linearly polarized electromagnetic field on resonance for either one- or two-photon couplings.
[27] The electromagnetic field energy density $\rho=\Delta E/V=I/c$; thus $I=h\nu/A\tau=(c\Delta E)/V=c^2h/\lambda V$. With $V=10^{-5}$ m^3 for the active part of the heat pipe oven we find $I_3=1.8\times10^{-5}$ W/m^2, $I_2=1.7\times10^{-6}$ W/m^2, and $I_1=9.9\times10^{-6}$ W/m^2. With $I=2n|\varepsilon|^2/Z_0$ and $Z_0=(\mu_0/\varepsilon_0)^{(1/2)}=376.7\ \Omega$ a ''noise'' field with the equivalent energy of one photon in the active part of the heat pipe oven has equivalent electric field amplitudes $|\varepsilon_3|=(Z_0I_3/2n)^{1/2}=0.058$ V/m, $|\varepsilon_2|=0.0178$ V/m, and $|\varepsilon_1|=0.0433$ V/m, which are used throughout.
[28] G. G. Padmabandu, G. R. Welch, I. N. Shubin, E. S. Fry, D. E. Nikonov, M. D. Lukin, and M. O. Scully, Phys. Rev. Lett. **76**, 2053 (1996).
[29] M. O. Scully, S. Y. Zhu, and A. Gavrielides, Phys. Rev. Lett. **62**, 2813 (1989).
[30] R. H. Dicke, Phys. Rev. **93**, 99 (1954); N. E. Rehler and J. H. Eberly, Phys. Rev. A **3**, 1735 (1971); L. Allen and J. H. Eberly, *Optical Resonance and Two Level Atoms* (Wiley, New York, 1975); R. L. Shoemaker, in *Laser and Coherence Spectroscopy*, edited by J. I. Steinfeld (Plenum, New York, 1978), p. 179.
[31] R. B. Miles and S. E. Harris, IEEE J. Quantum Electron. **QE-9**, 470 (1973).
[32] D. R. Bates and A. Damgaard, Philos. Trans. R. Soc. London, Ser. A **242**, 101 (1949); E. M. Anderson and V. A. Zilitis, Opt. Spectrosc. **16**, 99 (1964); H. Barry Bebb, Phys. Rev. **149**, 25 (1966); H. Eicher, IEEE J. Quantum Electron. **QE-11**, 121 (1975).
[33] W.-L. Wiese, M. W. Smith, and B. M. Miles, in *Atomic Transition Probabilities (Na-Ca)*, Natl. Bur. Stand. Ref. Data Ser., Natl. Bur. Stand. (U.S.) Circ. No. 22 (U.S. GPO, Washington, DC, 1969), Vol. II.